



The Orbit of NGC 5907 ULX-1

Andrea Belfiore¹, Ruben Salvaterra¹, Lara Sidoli¹, Gian Luca Israel², Luigi Stella², Andrea De Luca¹, Sandro Mereghetti¹, Paolo Esposito^{1,3}, Fabio Pintore⁴, Antonino D’Ai⁴, Guillermo Rodríguez Castillo⁴, Dominic J. Walton^{5,6}, Felix Fürst⁷, Danilo Magistrali⁸, Anna Wolter⁹, and Matteo Imbrogno^{2,10,11}

¹INAF, Istituto di Astrofisica Spaziale e Fisica Cosmica, Via Alfonso Corti 12, I-20133, Milano, Italy; andrea.belfiore@inaf.it

²INAF, Osservatorio Astronomico di Roma, Via Frascati 33, I-00078, Monteporzio Catone, Italy

³Scuola Universitaria Superiore IUSS Pavia, Palazzo del Broletto, Piazza Della Vittoria 15, I-27100, Pavia, Italy

⁴INAF, Istituto di Astrofisica Spaziale e Fisica Cosmica, Via Ugo La Malfa 153, I-90146, Palermo, Italy

⁵Centre for Astrophysics Research, University of Hertfordshire, College Lane, Hatfield AL10 9AB, UK

⁶Institute of Astronomy, University of Cambridge, Madingley Road, Cambridge CB3 0HA, UK

⁷European Space Agency (ESA), European Space Astronomy Centre (ESAC), Camino Bajo del Castillo s/n, 28692 Villanueva de la Cañada, Madrid, Spain

⁸Universidad Pontificia Comillas Madrid-ICAI, Calle de Alberto Aguilera 25, 28015, Madrid, Spain

⁹INAF, Osservatorio Astronomico di Brera, Via Brera 28, I-20121, Milano, Italy

¹⁰Dipartimento di Fisica, Università degli Studi di Roma “Tor Vergata,” via della Ricerca Scientifica 1, I-00133 Rome, Italy

¹¹Università degli Studi di Roma “La Sapienza,” Piazzale Aldo Moro 5, I-00185 Rome, Italy

Received 2023 December 22; revised 2024 February 23; accepted 2024 March 7; published 2024 April 9

Abstract

We report on the orbit of the binary system powering the most extreme ultraluminous X-ray pulsar known to date: NGC 5907 ULX-1 (hereafter ULX1). ULX1 has been the target of a substantial multi-instrument campaign, mainly in the X-ray band, but no clear counterparts are known in other bands. Although ULX1 is highly variable and pulsations can be transient (regardless of the source flux), the timing data collected so far allow us to investigate the orbit of this system. We find an orbital period $P_{\text{orb}} = 5.7_{-0.6}^{+0.1}$ days and a projected semi-axis $A_1 = 3.1_{-0.9}^{+0.8}$ lt-s. The most likely ephemeris is $P_{\text{orb}} = 5.6585(6)$ days, $A_1 = 3.1(4)$ lt-s, and the epoch of ascending nodes passage is $T_{\text{asc}} = 57751.37(5)$ MJD. However, there are six similar solutions acceptable within 3σ . We find further indications that ULX1 is a high-mass X-ray binary. This implies that we are observing its orbit face on, with an inclination $< 5^\circ$.

Unified Astronomy Thesaurus concepts: [Ultraluminous x-ray sources \(2164\)](#); [Orbit determination \(1175\)](#); [High mass x-ray binary stars \(733\)](#); [High time resolution astrophysics \(740\)](#)

1. Introduction

NGC 5907 ULX-1 (ULX1) is the most luminous member of the known ultraluminous X-ray pulsars (PULXs), peaking at an apparent luminosity of $L_{X,\text{peak}} \sim 10^{41}$ erg s⁻¹. PULXs are an emerging class of accreting X-ray pulsars with luminosity far in excess of the Eddington limit for a neutron star. This is a subclass of ultraluminous X-ray sources (ULXs), i.e., X-ray sources, located off center of their host galaxy, whose isotropic luminosity is greater than 10^{39} erg s⁻¹ (Walton et al. 2022; for recent reviews, see King et al. 2023; Pinto & Walton 2023; Tranin et al. 2024). PULXs are accreting pulsars, likely in high-mass X-ray binary (HMXB) systems, and thus are neutron stars orbiting a stellar companion. Their accretion geometry is not spherical, and their magnetic field is so strong that the Eddington limit—which assumes spherical symmetry and Thomson cross section—does not formally apply. Still, it remains a useful point of reference for comparison with other X-ray binary systems. Given the extreme nature of PULXs, it is important to investigate the nature of their companions and to measure the orbital parameters of these systems, as they reflect the conditions under which accretion at such extreme rates can occur. Because the detection of pulsations depends on several factors (including pulsed fraction, photon statistics, and background level), other known ULXs may yet turn out to be

PULXs as we keep observing them (King & Lasota 2016; Pintore et al. 2017; Walton et al. 2018).

After the discovery of pulsations with XMM-Newton and NuSTAR (Israel et al. 2017a), ULX1 has been regularly monitored with the Neil Gehrels Swift Observatory and observed on numerous occasions with XMM-Newton, NuSTAR, and Chandra (Fürst et al. 2023). The neutron star powering ULX1 shows strong long-term variability, exhibiting a high state that can last for years ($L_{X,\text{peak}} \sim 10^{41}$ erg s⁻¹), during which its flux is modulated over a period of 78 days (Walton et al. 2016), as well as a low state ($L_X < 10^{39}$ erg s⁻¹) during which a spatially extended X-ray nebula is revealed (which is otherwise drowned out by the emission from the point source; Belfiore et al. 2020). The source can transition between these high- and low-flux states within days (Walton et al. 2015). The pulsed fraction of ULX1 seems to vary randomly across different observations, and its spin period P_{spin} evolves noticeably, driven by the strong torque that results from the accretion of matter at a very high rate (which is also responsible for its extreme luminosity; Fürst et al. 2023). The earliest detection of pulsations revealed a spin period of 1.43 s in 2003, with the neutron star having subsequently been spun up to spin periods of 1.14 s in 2014 and 0.95 s in 2017. This erratic behavior hampers timing studies of the pulsar.

Because the host galaxy, NGC 5907, is nearly edge on, our line of sight to ULX1 is heavily obscured by dust. Optical/near-infrared searches for its counterpart have thus proven difficult. We are therefore forced to rely only on X-ray timing of the pulsar to infer the orbital parameters of this system. A



Original content from this work may be used under the terms of the [Creative Commons Attribution 4.0 licence](#). Any further distribution of this work must maintain attribution to the author(s) and the title of the work, journal citation and DOI.

Table 1
X-ray Observations Used in Our Analysis

Cluster	Obs. ID	Observatory	Date	Duration (ks)	Photons
A	0729561301	XMM-Newton	2014 Jul 9	42 (42)	12879
A	80001042002	NuSTAR	2014 Jul 9	57	3297
A	80001042004	NuSTAR	2014 Jul 12	56	3291
B	0804090301	XMM-Newton	2017 Jul 2	40 (32)	3394
B	0804090401	XMM-Newton	2017 Jul 4	36 (36)	2221
C	0824320201	XMM-Newton	2019 Jun 12	60 (59)	12216
C	0824320301	XMM-Newton	2019 Jun 19	49 (49)	9069
C	0824320401	XMM-Newton	2019 Jun 26	64 (54)	7854

Note. For XMM-Newton, in parentheses is the net exposure time, after the removal of high background periods. The number of photons is measured after all filters have been applied. The baselines for the three clusters are 404 ks for cluster A, 222 ks for cluster B, and 1271 ks for cluster C.

first estimate of the period (P_{orb}), projected semi-axis ($A_1 = a_{\text{ns}} \cdot \sin i$), and epoch of ascending nodes (T_{asc}) of the orbit of the neutron star came together with the discovery of pulsations (Israel et al. 2017a). Such an analysis was based on two NuSTAR observations taken in 2014 July, with a baseline of 4.7 days. They report, at 1σ confidence, $P_{\text{orb}} = 5.3_{-0.9}^{+2.0}$ days and $A_1 = 2.5_{-0.8}^{+4.3}$ lt-s. However, at 3σ confidence, only lower limits on $A_1 > 1.4$ lt-s and $P_{\text{orb}} > 4.0$ days were obtained, whereas upper limits rely on physical considerations about the mass of the companion.

In this paper we consider all of the observations taken so far with XMM-Newton and NuSTAR and derive an updated orbital ephemeris. Section 2 describes the data used for this paper and how they were selected. Section 3 describes the timing analysis that leads to our results, presented in Section 4. A discussion follows in Section 5, and conclusions are drawn in Section 6.

2. Observations and Data Preparation

Timing ULX1 requires sufficient photon statistics and good time resolution, which restricts our analysis to the data obtained by two X-ray observatories: NuSTAR (Harrison et al. 2013) and XMM-Newton (Jansen et al. 2001). The rapid and erratic spin evolution of ULX1 does not allow for coherent timing on long timescales (more than a few weeks), while on short timescales, the intrinsic behavior of the pulsar (e.g., the accretion-driven spin-up) can account for any linear trend in spin period. Therefore, we must rely on clusters of two or more observations, all taken within a couple of weeks of each other, during which pulsations are detected. Any nonlinearity in the spin evolution within each observation cluster can be ascribed, to a first approximation, to the orbit of the system.

So far, three clusters of observations that meet the above requirements are available (see Table 1): three observations in 2014 (cluster A; these are the data that led to the initial discovery of pulsations and to the first orbital ephemeris), two observations in 2017 (cluster B), and three observations in 2019 (cluster C).

The XMM-Newton observations were taken with the the EPIC-PN camera (Strüder et al. 2001) in full frame mode and thus have a time resolution of 73.4 ms. We do not consider the EPIC-MOS data because its time resolution is not sufficient for

the timing analysis of a ~ 1 s pulsar. We used the XMM-Newton Scientific Analysis System (v21.0; Gabriel et al. 2004) to reprocess and filter the events and to correct their time of arrival to the solar system barycenter (using the DE200 ephemeris). We adopt the position obtained for ULX1 with Chandra (Sutton et al. 2013): R. A. = $15^{\text{h}}15^{\text{m}}58^{\text{s}}.62 \pm 0^{\text{s}}.01$, decl. = $+56^{\circ}18'10''.3 \pm 0''.1$ (J2000). We applied standard quality filters and excluded periods of high background, as recommended by the XMM-Newton team. We kept all the events within $30''$ of the position of ULX1 with energies $E > 1$ keV. These criteria maximize the strength of the pulsed signal for this particular pulsar (Israel et al. 2017a).

The NuSTAR observations used data from both focal plane modules (FPMA and FPMB), which have a time resolution of $2\ \mu\text{s}$. They were reduced with the NuSTAR Data Analysis Software (NuSTARDAS v2.1.2). We applied the standard quality filters recommended by the NuSTAR team and kept all the events within $49''$ of the position of ULX1 with energies in the 3–15 keV range.

We again shifted the time of arrival of the photons to the solar system barycenter.

3. Data Analysis

The pulse profile of ULX1 is well approximated by a sinusoid. We construct a model for the evolution of the period of this sinusoid and fit it directly to the time of arrival of each photon, using an unbinned likelihood analysis (supplemental material in Israel et al. 2017a). The most likely set of parameters in our model is our best-fit solution. We then perturb the optimal solution by varying each single parameter. As we shift one parameter, we profile the likelihood by maximizing it over all the other parameters. We then estimate the uncertainties by measuring the drop in likelihood and applying Wilks’s theorem (Cowan et al. 2011).

Our model accounts for an evolution of the intrinsic spin period of the pulsar (due to accretion or other torques) and the Doppler modulation induced by the orbital motion. We assume that within each cluster of observations (taken less than 2 weeks apart) the intrinsic evolution of the spin period P is linear, i.e., its time derivative \dot{P} is constant. We do not assume any relation between the spin parameters taken in different clusters of observations as the accretion rate is variable and

hardly predictable. Any nonlinearity in the spin evolution observed within a cluster of observations is ascribed to the orbital modulation. We assume that the orbit is circular and that its parameters (the projected semi-axis A_1 , the orbital period P_{orb} , and the epoch of ascending node passage T_{asc}) do not change across different clusters.

Our assumption of a circular orbit is not granted a priori. However, we can take it as a first-order approximation. In particular, because most often the pulsar is far from periapsis, we expect a very limited bias due to this assumption. As more timing data become available, this model can be extended to account for an eccentric orbit.

It is clear that the secular spin evolution is intrinsic because no orbit (not even around a supermassive black hole) could account for a change in the spin period of $>10\%$, as observed for ULX1 (Fürst et al. 2023). However, on short timescales, the shift in \dot{P} induced by a binary orbit can be of the same order as the intrinsic \dot{P} . Therefore, this observable is fully degenerate with the unknown intrinsic spin-up (or spin-down), and we cannot build upon that to constrain the orbit.

We start by considering each cluster of observations by itself. This analysis provides weak independent constraints on the three orbital parameters. In order to minimize the correlation between P_{orb} and T_{asc} , we keep T_{asc} as close as possible to the midpoint of each cluster. We focus on A_1 and P_{orb} by comparing their estimates in each set of observations and combining them. The analysis of each cluster maximizes the likelihood over all the other parameters: P , \dot{P} , and the orbital phase T_{asc} .

Afterwards, we shift our estimates of T_{asc} to a common epoch (close to the midpoint of all data) by adding or subtracting an integer number of full orbits. Generally, given a pair A_1 and P_{orb} , the values of T_{asc} shifted from clusters A and C do not match. Forcing them to be the same, while considering both data sets at once, introduces some aliases in P_{orb} separated by

$$\Delta P_{\text{orb}} \simeq \frac{P_{\text{orb}}^2}{T_C - T_A} \simeq 0.018 \text{ days.} \quad (1)$$

Finally, we examine all these aliases, considering data from all three clusters at the same time.

4. Results

The likelihood analysis within each cluster of observations provides nonlinear constraints on the orbital parameters. In particular, only clusters A and C provide independent estimates of all the three orbital parameters. The analysis of cluster B, which has a much shorter baseline, provides looser constraints, in which each of the orbital parameters is fully degenerate with the other two. Therefore, we used only the analysis of clusters A and C to derive a first estimate for A_1 and P_{orb} (see Figure 1).

We then combined the two estimates of A_1 and P_{orb} , without enforcing coherence in the orbital phase between the two epochs. The most likely values are $P_{\text{orb}} = 5.66$ days and $A_1 = 3.10$ lt-s and, at 3σ , $5.0 \text{ days} < P_{\text{orb}} < 5.8 \text{ days}$ and $2.3 \text{ lt-s} < A_1 < 4.0 \text{ lt-s}$. These values are consistent to within 1σ with the individual estimates obtained for each of the clusters when considered independently (again, see Figure 1). Therefore, our approximation with a circular orbit seems to be justified.

Finally, we fixed the orbital phase between the two main clusters, A and C, and also incorporated the data from cluster

B. As described above, in Section 3, forcing the coherence in orbital phase between clusters A and C induces aliases in P_{orb} . Many of these aliases can be ruled out as they imply a value of T_{asc} , which is not consistent with the observations in cluster B. Only seven aliases are acceptable to within 3σ , and one of them stands out (ID 320, corresponding to 320 full orbits between T_A and T_C ; see Table 2).

The most likely value of the orbital parameters, for alias 320, is $P_{\text{orb}} = 5.6585(6)$ days, $A_1 = 3.1(4)$ lt-s, and $T_{\text{asc}} = \text{MJD } 57751.37(5)$. The reported uncertainty, at 3σ on a single parameter of interest, is in parentheses after the last digit. As noted previously, T_{asc} is taken close to the midpoint of the observing baseline, minimizing the correlation between P_{orb} and T_{asc} . The correlation between P_{orb} and A_1 does not depend on our choice of T_{asc} (see Figure 2).

From these constraints, we can derive some other parameters of the system and its geometry: the Roche lobe radius and the inclination of the orbital plane. These parameters depend on the mass of the neutron star, M_{ns} , and the mass of its companion $M_c = q \cdot M_{\text{ns}}$ (where q is the mass ratio of the binary components). We take three representative values of $M_{\text{ns}} = 1.4, 1.8,$ and $2.2 M_{\odot}$ and plot these quantities for a range of M_c (see Figure 3). We note that the dependence of our results on M_{ns} is very weak. For $M_{\text{ns}} = 1.8 M_{\odot}$, we indicate with a shaded band the uncertainty, at 3σ , considering any of the seven acceptable aliases in P_{orb} .

We estimate the Roche lobe radius R_l from the semimajor axis of the orbit, a , obtained from P_{orb} through Kepler's third law:

$$R_l = f(q) \cdot \left(\frac{GM_{\text{ns}}}{4\pi^2} \right)^{\frac{1}{3}} (1+q)^{\frac{1}{3}} P_{\text{orb}}^{\frac{2}{3}} \\ \simeq 2.062 \frac{q^{\frac{2}{3}}(1+q)^{\frac{1}{3}}}{0.6q^{\frac{2}{3}} + \ln(1+q^{\frac{1}{3}})} \left(\frac{M_{\text{ns}}}{M_{\odot}} \right)^{\frac{1}{3}} \left(\frac{P_{\text{orb}}}{\text{days}} \right)^{\frac{2}{3}} R_{\odot}, \quad (2)$$

where we adopted the approximation $R_l \simeq f(q) \cdot a$ (Eggleton 1983). The upper panel of Figure 3 shows the relation $R_l(M_c)$ for our estimate of P_{orb} .

We infer the inclination i of the orbital plane with respect to the line of sight by comparing a , obtained from P_{orb} , and the observed $A_1 = \frac{q}{1+q} a \sin i$:

$$\sin i = \left(\frac{GM_{\text{ns}}}{4\pi^2} \right)^{-\frac{1}{3}} \frac{(1+q)^{\frac{2}{3}}}{q} P_{\text{orb}}^{-\frac{2}{3}} A_1 \\ = 0.102 \frac{(1+q)^{\frac{2}{3}}}{q} \left(\frac{M_{\text{ns}}}{M_{\odot}} \right)^{-\frac{1}{3}} \left(\frac{P_{\text{orb}}}{\text{days}} \right)^{-\frac{2}{3}} \left(\frac{A_1}{\text{lt-s}} \right). \quad (3)$$

The lower panel of Figure 3 shows the relation $i(M_c)$ for our estimate of P_{orb} and A_1 . The lack of eclipses or dips in the light curve of ULX1, instead observed for M51 ULX7 (Hu et al. 2021; Vasilopoulos et al. 2021), implies that $\sin i < \sqrt{1 - f^2(q)}$; hence, $i < 78^\circ$. If $M_c > 5 M_{\odot}$, then the orbit must be nearly face on, with $i < 5^\circ$.

5. Discussion

We have undertaken a multi-epoch X-ray analysis of the ULX pulsar ULX1 in order to place updated constraints on its orbital parameters by means of X-ray timing. This information is key to understanding the nature of this remarkable binary system and can only be accessed via such studies in the X-ray band given

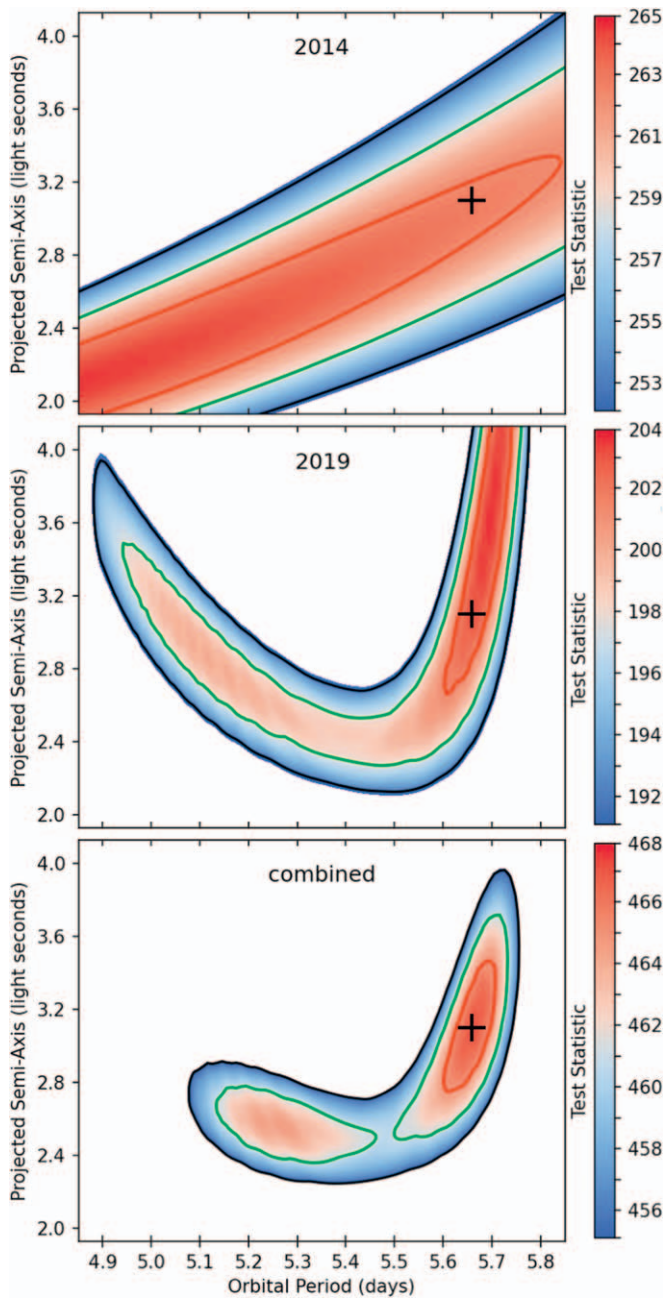


Figure 1. Estimates of the orbital period (P_{orb} , on the X-axis) and the projected semi-axis (A_1 , on the Y-axis) of the orbit of ULX1. These estimates are profiled over the orbital phase (T_{asc}). The upper panel comes from the observation cluster A, the central panel from the observation cluster C, and the bottom panel combines the above two estimates (without fixing T_{asc} between them). Some aliasing is visible in the central panel (propagated to the bottom panel). A black cross marks the most likely value of $P_{\text{orb}} = 5.66$ days and $A_1 = 3.10$ lt-s, from the combined estimate shown in the bottom panel. Level curves indicate the 1σ (red), 2σ (green), and 3σ (black) regions, for 2 degrees of freedom.

that the distance to the source and the level of obscuration toward it have prevented the detection of any stellar counterpart at other wavelengths (e.g., Heida et al. 2019). Using our updated constraints for ULX1, we start by comparing its orbital and spin period (P_{orb} and P_{spin} , respectively) with those of other X-ray binaries containing a pulsar (Corbet 1984); see Figure 4. We also included in the plot the other PULXs with a firm estimate of their orbital period: M82 X-2 (Bachetti et al. 2014); M51 ULX-7 (Rodríguez Castillo et al. 2020); NGC 7793 P13

(Fürst et al. 2016; Israel et al. 2017b; Fürst et al. 2021); Swift J0243.6 + 6124 (Tsygankov et al. 2018; Wilson-Hodge et al. 2018); RX J0209.6-7427 (Chandra et al. 2020; Vasilopoulos et al. 2020; Hou et al. 2022); and SMC X-3 (Townsend et al. 2017; Liu et al. 2022).

Although this plot cannot convey the full complexity of the behavior of these sources, it captures some traits that distinguish different classes of objects (color-coded in Figure 4). These are classified by looking at the companion and considering a broader set of parameters, like luminosity and variability, spectral shape/features, orbital shape and spin-up (see Chaty 2022 for a recent review). Low-mass X-ray binaries have donors with mass $M_d < 1 M_{\odot}$ and are mostly found to have compact orbits and the accretors spin at high rates. HMXBs have donors with mass $M_d > 5 M_{\odot}$; their orbits are larger and the accretors generally have longer spin periods. PULXs are in the central region of the Corbet diagram, on the lower end of P_{spin} and P_{orb} of HMXBs.

The PULXs neighboring ULX1 in the Corbet diagram are M82 X-2 and M51 ULX-7, which are both known to be HMXBs. M82 X-2 has a mass function $f(M) > 5.2 M_{\odot}$ (Bachetti et al. 2014). M51 ULX-7 has a mass function $f(M) > 8 M_{\odot}$, (Rodríguez Castillo et al. 2020) and candidate OB supergiant (OBsg) counterparts (Earnshaw et al. 2016). Their variability patterns show some similarity to ULX1 although they are fainter. Other PULXs, like the Galactic Swift J0243.6 + 6124 and RX J0209.6-7427 have larger P_{orb} and P_{spin} . Both of them have a Be companion and show a markedly different variability pattern: they show a burst at periastron, and occasionally this burst can briefly surpass the limit of $10^{39} \text{ erg s}^{-1}$ (i.e., they do not exhibit these extreme luminosities for extended periods, in contrast to ULX1 and many of the other ULX pulsars).

Exploring the other pulsar binaries with parameters similar to ULX1, we find that these are generally interpreted as HMXBs accreting through a disk. The formation of a disk demands a compact orbit and therefore a short P_{orb} (Tauris & van den Heuvel 2023). A disk is required to attain a very large secular spin-up and to reach a short P_{spin} . This explains their behavior, common also to M82 X-2 and M51 ULX-7: persistent high luminosity and strong spin-up over long periods.

Indeed, the closest source to ULX1 is SMC X-1, an HMXB thought to be disk fed, with a spin period $P_{\text{spin}} = 0.71$ s, an orbital period $P_{\text{orb}} = 3.89$ days, and a B0 supergiant companion (Falanga et al. 2015). It is variable, its luminosity can reach up to the Eddington limit, and it spins up constantly over several years (Brumback et al. 2022). Its pulsations are transient even in a high state, just like ULX1 (Pike et al. 2019). Two other peculiar sources are also close to ULX1 in the Corbet diagram: Her X-1, with a $2 M_{\odot}$ donor, and GRO J1744-28, known for its peculiar bursting behavior. However, they are both accreting below their Eddington limits, and their phenomenology does not match that of ULX1.

Our estimate of P_{orb} , the known $P_{\text{spin}} \sim 1$ s, and the analogy with similar systems lead us to interpret ULX1 as an HMXB, potentially with an OBsg companion, accreting through a disk onto a neutron star. This interpretation is consistent with the size of the Roche lobe inferred in Equation (2) (see Figure 3). A main-sequence star would severely underfill its Roche lobe given the orbital parameters we find for ULX1. A red giant could fill its Roche lobe if it has a core mass $> 0.195 M_{\odot}$ (Rappaport et al. 1995). However, a highly super-Eddington

Table 2
Coherent Orbital Solutions Acceptable at the 3σ Level in a Single Parameter

ID	TS	N_σ	R_A	R_B	R_C	P_{orb} (days)	A_1 (lt-s)	T_{asc} (MJD)
320	543.83	...	262.76	76.53	202.92	5.6585(6)	3.1(4)	57751.37(5)
343	541.53	1.5	263.80	76.78	199.32	5.2753(3)	2.5(3)	57753.65(5)
338	540.11	1.9	263.19	76.79	198.51	5.3538(3)	2.5(3)	57751.05(5)
348	539.41	2.1	263.13	75.55	199.12	5.1992(2)	2.6(2)	57750.97(4)
325	539.36	2.1	262.09	75.98	199.68	5.5702(4)	2.7(3)	57754.06(4)
333	536.21	2.7	262.00	74.71	197.90	5.4348(2)	2.5(1)	57753.83(3)
351	535.05	2.9	261.88	73.50	198.10	5.1546(1)	2.7(1)	57753.52(1)

Note. The ID corresponds to the number of full orbits between the observations in clusters A and C. The drop in test statistic (TS) from the optimum solution asymptotically follows a χ^2 distribution with 1 degree of freedom and is converted to σ units (i.e., N_σ). We report also the Rayleigh TS (a measure of the strength of the signal) for each cluster of observations (R_A , R_B , and R_C). The orbital parameters are the orbital period P_{orb} , the projected semi-axis A_1 , and the epoch of ascending nodes T_{asc} . All the uncertainties (in parentheses after the last digit) are at 3σ on a single parameter, with respect to the most likely solution (ID 320).

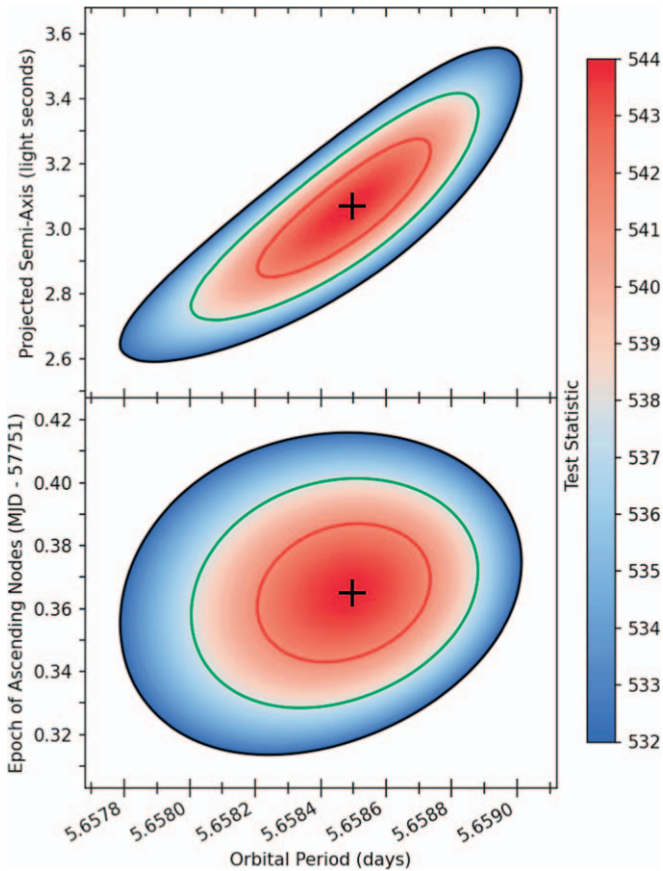


Figure 2. Estimates of the orbital parameters for the most likely alias (ID 320 in Table 2) in the orbital period (P_{orb} , on the X-axis) for ULX1 based on our final, combined analysis. The upper panel shows the projected semi-axis (A_1) on the Y-axis. The lower panel shows the epoch of passage of the ascending nodes (T_{asc}) on the Y-axis. The black cross marks the most likely orbital ephemeris. Level curves indicate the 1σ (red), 2σ (green), and 3σ (black) regions, for 2 degrees of freedom.

regime (exceeding the Eddington limit by a factor ~ 30) can only be sustained if $P_{\text{orb}} \simeq 1$ day (Rappaport & Joss 1997). Therefore, unless a much more efficient configuration can be devised, which is also compatible with $P_{\text{orb}} \simeq 5.7$ days, a red giant companion is ruled out. OBsg and Be companions to

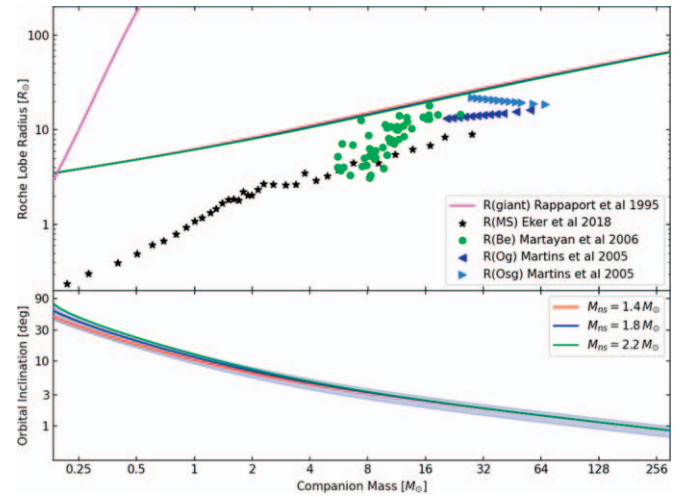


Figure 3. Geometrical parameters of the ULX1 system for three values of the mass of the neutron star ($M_{\text{ns}} = 1.4$, 1.8 , and $2.2 M_\odot$, red, blue, and green lines, respectively) depending on the mass of the companion, M_c , on the X-axis. Shaded regions cover the 3σ uncertainty ranges on the orbital parameters, assuming $M_{\text{ns}} = 1.8 M_\odot$. Upper panel: on the Y-axis is the Roche lobe radius R_l in solar radius units (see Equation (2)). Stellar radii (R_{star}) are also reported for different masses and stellar types for comparison (data from Rappaport et al. 1995; Martins et al. 2005; Martayan et al. 2006; Eker et al. 2018). For mass transfer to occur, $R_{\text{star}} \simeq R_l$. This rules out a main-sequence companion. Lower panel: on the Y-axis is the system inclination (see Equation (3)). Unless M_c is very low, the orbit is \sim face on.

ULX1 could fill their Roche lobes, being largely affected by factors such as rotation, metallicity, and magnetic field. A stable super-Eddington regime in which mass is transferred on a nuclear timescale can indeed be sustained for a supergiant companion, provided that its outer layer has a large metallicity gradient (Quast et al. 2019). This is consistent with the timescale required to fill up a nebula with hot plasma, which can explain the diffuse emission observed around ULX1 (Belfiore et al. 2020).

6. Conclusion

We have used all the available X-ray data on ULX1 to extract an updated orbital ephemeris. We analyzed groups of observations clustered in time, initially without enforcing

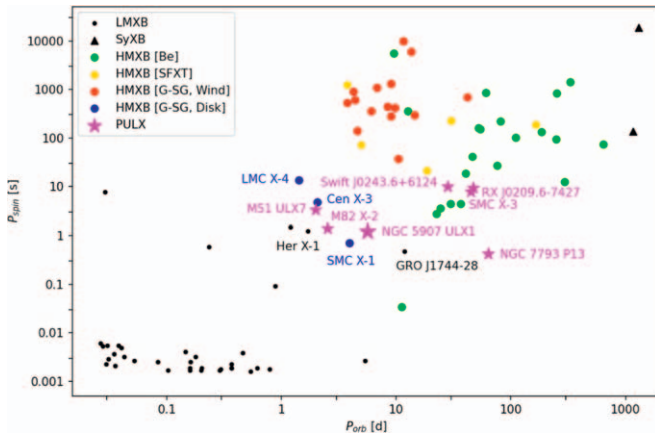


Figure 4. Distribution of the orbital period (P_{orb} , in days, on the X-axis) vs. spin period (P_{spin} , in seconds, on the Y-axis) for known pulsars in X-ray binaries. The data shown are from Liu et al. (2005), Avakyan et al. (2023), Fortin et al. (2023), Neumann et al. (2023), and Esposito et al. (2016). Symbols and colors correspond to the legend, where SyXB indicates symbiotic X-ray binaries and SFXT indicates supergiant fast X-ray transients. We labeled all the PULXs that currently have a firm estimate of P_{orb} as well as some other systems that lie at a position close to that of ULX1 in this diagram.

coherence in the orbital phase between them. We estimated the orbital period as $P_{\text{orb}} = 5.7_{-0.6}^{+0.1}$ days and the projected semi-axis as $A_1 = 3.1_{-0.9}^{+0.8}$ lt-s. This improves on the previous estimate by Israel et al. (2017a) where, at the same confidence level, only lower limits were given. Therefore, as already suspected, the 78 day periodicity of ULX1 (Walton et al. 2016) is not an orbital modulation.

We subsequently tried to work out a complete ephemeris by enforcing coherence in the orbital phase between groups of observations. We found seven solutions, mutually exclusive, that are compatible with our measure of P_{orb} and A_1 reported above. The most likely ephemeris is $P_{\text{orb}} = 5.6585(6)$ days, $A_1 = 3.1(4)$ lt-s, and epoch of ascending nodes passage $T_{\text{asc}} = 57751.37(5)$ MJD. A specific ephemeris is needed to assign an orbital phase to each observation, enabling future phase-resolved analyses of the available data. To resolve the remaining ambiguity over the precise orbital parameters, new and carefully devised timing observations are needed. Any new independent ephemeris would provide a measure of the evolution of P_{orb} , as already done for several other HMXBs (Falanga et al. 2015) and recently also claimed for M82 X-2 (Bachetti et al. 2022). Because the orbital decay increases with

the mass-loss rate of the donor (Quast et al. 2019), temporal baselines comparable to the existing coverage could be sufficient to detect these changes.

Based on our updated results for its orbit, we argue that ULX1 is an HMXB that contains a neutron star accreting at extreme rates through a disk from an OBsg donor. This implies that the orbit is nearly face on with an inclination $i < 5^\circ$.

Acknowledgments

We acknowledge financial support from ASI under ASI/INAF agreement N.2017-14.H.O. G.L.I., P.E., F.P., A.D.A., G.R.C., and A.W. acknowledge financial support from the Italian Ministry for University and Research through the PRIN grant 2022Y2T94C (SEAWIND) and the INAF LG 2023 BLOS-SOM. A.D.A. acknowledges funding from the Italian Space Agency, contract ASI/INAF n. I/004/11/4. S.M. acknowledges support from the Italian Ministry for University and Research, through grant 2017LJ39LM (UNIAM) and from INAF through a Large Program for Fundamental Research 2022. F.P. acknowledges financial support from the Italian Ministry for University and Research through the grant 2023 (OBIWAN). M.I. is supported by the AASS Ph.D. joint research programme between the University of Rome “La Sapienza” and the University of Rome “Tor Vergata,” with the collaboration of the National Institute of Astrophysics (INAF). This research is based on observations obtained with XMM-Newton, a European Space Agency (ESA) science mission with instruments and contributions directly funded by ESA member states and NASA. This work also made use of data from NuSTAR, a mission led by the California Institute of Technology, managed by the Jet Propulsion Laboratory, and funded by NASA.

Appendix

Orbital Parameters for All the Acceptable Ephemerides

The main text includes a plot (Figure 2) that shows the correlation between the orbital parameters for the most likely orbital ephemeris (which we refer to as ID 320). We report here similar plots for all the other ephemerides listed in Table 2, which, while less likely, are all formally acceptable within the 3σ level when compared against the best-fit solution (see Figures 5 and 6). All the contour levels refer to the most likely ephemeris, displayed in Figure 2, and therefore share the same color bar.

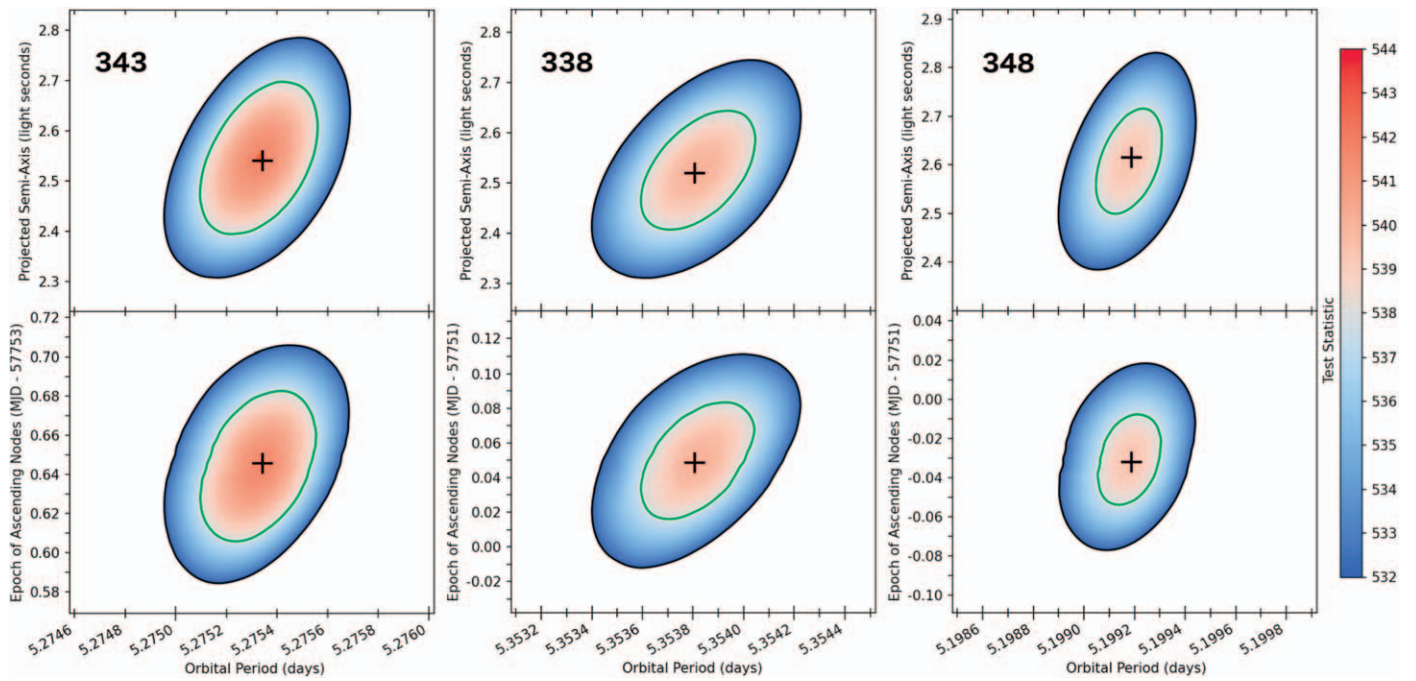


Figure 5. Estimates of the orbital parameters for the aliases labeled with IDs 343, 338, and 348 in Table 2, from left to right. See Figure 2 for more details.

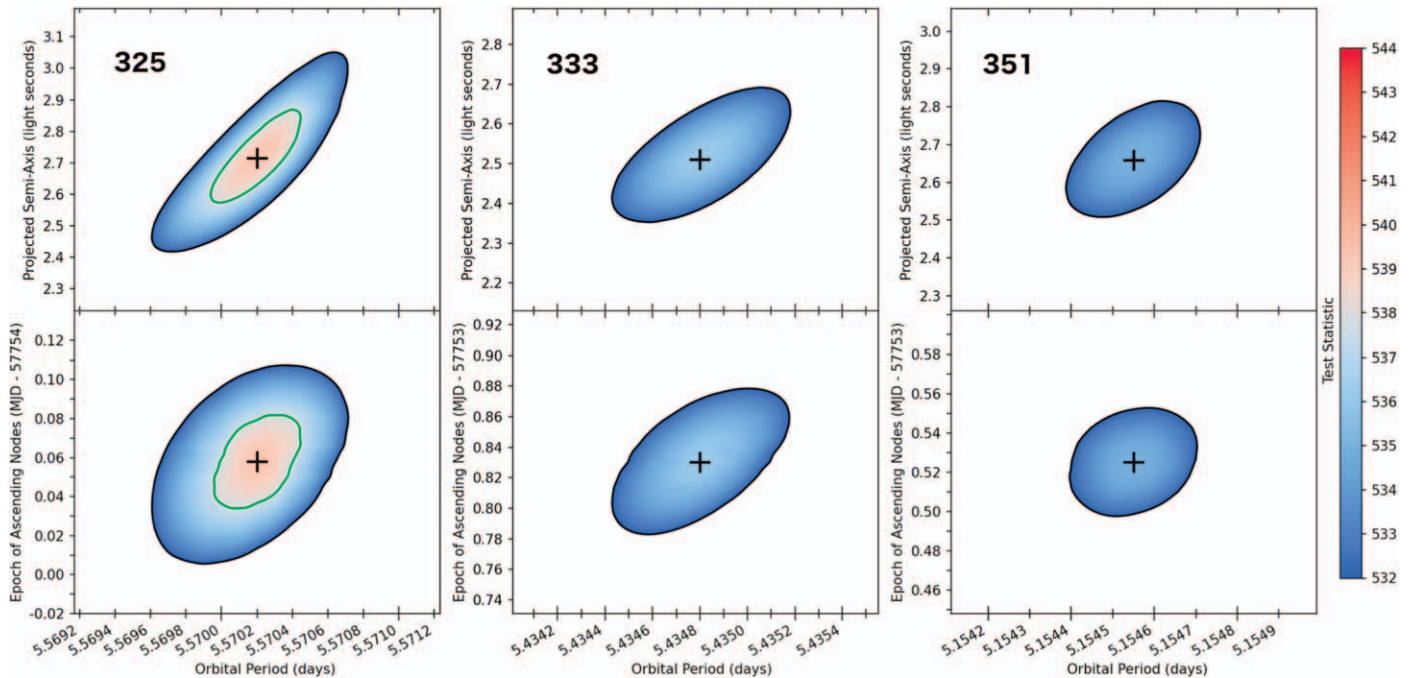





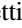




Figure 6. Estimates of the orbital parameters for the aliases labeled with IDs 325, 333, and 351 in Table 2, from left to right. See Figure 2 for more details.

ORCID iDs

Andrea Belfiore  <https://orcid.org/0000-0002-2526-1309>
 Ruben Salvaterra  <https://orcid.org/0000-0002-9393-8078>
 Lara Sidoli  <https://orcid.org/0000-0001-9705-2883>
 Gian Luca Israel  <https://orcid.org/0000-0001-5480-6438>
 Luigi Stella  <https://orcid.org/0000-0002-0018-1687>
 Andrea De Luca  <https://orcid.org/0000-0001-6739-687X>
 Sandro Mereghetti  <https://orcid.org/0000-0003-3259-7801>
 Paolo Esposito  <https://orcid.org/0000-0003-4849-5092>

Fabio Pintore  <https://orcid.org/0000-0002-3869-2925>
 Antonino D’Ai  <https://orcid.org/0000-0002-5042-1036>
 Guillermo Rodríguez Castillo  <https://orcid.org/0000-0003-3952-7291>
 Dominic J. Walton  <https://orcid.org/0000-0001-5819-3552>
 Felix Fürst  <https://orcid.org/0000-0003-0388-0560>
 Danilo Magistrali  <https://orcid.org/0000-0001-6337-2184>
 Anna Wolter  <https://orcid.org/0000-0001-5840-9835>
 Matteo Imbrogno  <https://orcid.org/0000-0001-8688-9784>

References

- Avakyan, A., Neumann, M., Zainab, A., et al. 2023, *A&A*, 675, A199
- Bachetti, M., Harrison, F. A., Walton, D. J., et al. 2014, *Natur*, 514, 202
- Bachetti, M., Heida, M., Maccarone, T., et al. 2022, *ApJ*, 937, 125
- Belfiore, A., Esposito, P., Pintore, F., et al. 2020, *NatAs*, 4, 147
- Brumback, M. C., Grefenstette, B. W., Buisson, D. J. K., et al. 2022, *ApJ*, 926, 187
- Chandra, A. D., Roy, J., Agrawal, P. C., & Choudhury, M. 2020, *MNRAS*, 495, 2664
- Chaty, S. 2022, *Accreting Binaries; Nature, Formation, and Evolution* (Bristol: IOP Publishing)
- Corbet, R. H. D. 1984, *A&A*, 141, 91
- Cowan, G., Cranmer, K., Gross, E., & Vitells, O. 2011, *EPJC*, 71, 1554
- Earnshaw, H. M., Roberts, T. P., Heil, L. M., et al. 2016, *MNRAS*, 456, 3840
- Eggleton, P. P. 1983, *ApJ*, 268, 368
- Eker, Z., Bakış, V., Bilir, S., et al. 2018, *MNRAS*, 479, 5491
- Esposito, P., Israel, G. L., Belfiore, A., et al. 2016, *MNRAS*, 457, L5
- Falanga, M., Bozzo, E., Lutovinov, A., et al. 2015, *A&A*, 577, A130
- Fortin, F., García, F., Simaz Bunzel, A., & Chaty, S. 2023, *A&A*, 671, A149
- Fürst, F., Walton, D. J., Harrison, F. A., et al. 2016, *ApJL*, 831, L14
- Fürst, F., Walton, D. J., Heida, M., et al. 2021, *A&A*, 651, A75
- Fürst, F., Walton, D. J., Israel, G. L., et al. 2023, *A&A*, 672, A140
- Gabriel, C., Denby, M., Fyfe, D. J., et al. 2004, in *ASP Conf. Ser.* 314, *Astronomical Data Analysis Software and Systems (ADASS) XIII*, ed. F. Ochsenbein, M. G. Allen, & D. Egret (San Francisco, CA: ASP), 759
- Harrison, F. A., Craig, W. W., Christensen, F. E., et al. 2013, *ApJ*, 770, 103
- Heida, M., Harrison, F. A., Brightman, M., et al. 2019, *ApJ*, 871, 231
- Hou, X., Ge, M. Y., Ji, L., et al. 2022, *ApJ*, 938, 149
- Hu, C.-P., Ueda, Y., & Enoto, T. 2021, *ApJ*, 909, 5
- Israel, G. L., Belfiore, A., Stella, L., et al. 2017a, *Sci*, 355, 817
- Israel, G. L., Papitto, A., Esposito, P., et al. 2017b, *MNRAS*, 466, L48
- Jansen, F., Lumb, D., Altieri, B., et al. 2001, *A&A*, 365, L1
- King, A., & Lasota, J.-P. 2016, *MNRAS*, 458, L10
- King, A., Lasota, J.-P., & Middleton, M. 2023, *NewAR*, 96, 101672
- Liu, J., Vasilopoulos, G., Ge, M., et al. 2022, *MNRAS*, 517, 3354
- Liu, Q. Z., van Paradijs, J., & van den Heuvel, E. P. J. 2005, *A&A*, 442, 1135
- Martayan, C., Frémat, Y., Hubert, A. M., et al. 2006, *A&A*, 452, 273
- Martins, F., Schaerer, D., & Hillier, D. J. 2005, *A&A*, 436, 1049
- Neumann, M., Avakyan, A., Doroshenko, V., & Santangelo, A. 2023, *A&A*, 677, A134
- Pike, S. N., Harrison, F. A., Bachetti, M., et al. 2019, *ApJ*, 875, 144
- Pinto, C., & Walton, D. J. 2023, arXiv:2302.00006
- Pintore, F., Zampieri, L., Stella, L., et al. 2017, *ApJ*, 836, 113
- Quast, M., Langer, N., & Tauris, T. M. 2019, *A&A*, 628, A19
- Rappaport, S., & Joss, P. C. 1997, *ApJ*, 486, 435
- Rappaport, S., Podsiadlowski, P., Joss, P. C., Di Stefano, R., & Han, Z. 1995, *MNRAS*, 273, 731
- Rodríguez Castillo, G. A., Israel, G. L., Belfiore, A., et al. 2020, *ApJ*, 895, 60
- Strüder, L., Briel, U., Dennerl, K., et al. 2001, *A&A*, 365, L18
- Sutton, A. D., Roberts, T. P., Gladstone, J. C., et al. 2013, *MNRAS*, 434, 1702
- Tauris, T. M., & van den Heuvel, E. P. J. 2023, *Physics of Binary Star Evolution. From Stars to X-ray Binaries and Gravitational Wave Sources* (Princeton, NJ: Princeton Univ. Press)
- Townsend, L. J., Kennea, J. A., Coe, M. J., et al. 2017, *MNRAS*, 471, 3878
- Tranin, H., Webb, N., Godet, O., & Quintin, E. 2024, *A&A*, 681, A16
- Tsygankov, S. S., Doroshenko, V., Mushtukov, A. A., Lutovinov, A. A., & Poutanen, J. 2018, *MNRAS*, 479, L134
- Vasilopoulos, G., Koliopanos, F., Haberl, F., et al. 2021, *ApJ*, 909, 50
- Vasilopoulos, G., Ray, P. S., Gendreau, K. C., et al. 2020, *MNRAS*, 494, 5350
- Walton, D. J., Fürst, F., Bachetti, M., et al. 2016, *ApJL*, 827, L13
- Walton, D. J., Fürst, F., Heida, M., et al. 2018, *ApJ*, 856, 128
- Walton, D. J., Harrison, F. A., Bachetti, M., et al. 2015, *ApJ*, 799, 122
- Walton, D. J., Mackenzie, A. D. A., Gully, H., et al. 2022, *MNRAS*, 509, 1587
- Wilson-Hodge, C. A., Malacaria, C., Jenke, P. A., et al. 2018, *ApJ*, 863, 9